Ultradeep fused silica glass etching with an HF-resistant photosensitive resist for optical imaging applications

John M Nagarah and Daniel A Wagenaar

Broad Fellows Program and Division of Biology
California Institute of Technology
1200 E. California Blvd.
MC 216-76
Pasadena, CA 91125

jnagarah@caltech.edu
daw@caltech.edu

Abstract

Microfluidic and optical sensing platforms are commonly fabricated in glass and fused silica (quartz) because of their optical transparency and chemical inertness. Hydrofluoric acid (HF) solutions are the etching media of choice for deep etching into silicon dioxide substrates, but processing schemes become complicated and expensive for etching times greater than 1 hour due to the aggressiveness of HF migration through most masking materials. We present here etching into fused silica more than 600 μm deep while keeping the substrate free of pits and maintaining a polished etched surface suitable for biological imaging. We utilize an HF-resistant photosensitive resist (HFPR) which is not attacked in 49% HF solution. Etching characteristics are compared for substrates masked with the HFPR alone and the HFPR patterned on top of Cr/Au and polysilicon masks. We used this etching process to fabricate suspended fused silica membranes, 8–16 μm thick, and show that imaging through the membranes does not negatively affect image quality of fluorescence microscopy of biological tissue. Finally, we realize small through-pore arrays in the suspended membranes. Such devices will have applications in planar electrophysiology platforms, especially where optical imaging is required.

1. Introduction

Glass and fused silica are appealing materials for constructing microelectromechanical systems (MEMS), lab-on-a-chip, and microfluidic platforms due to their chemical inertness, biocompatibility, optical transparency, mechanical rigidity, high melting point, electrical insulation, gas impermeability, and ability to bond to silicon, glass, and polydimethylsiloxane (PDMS) [1-3]. However, many of the wafer-scale processing methods developed for silicon are not readily transferable to glass; hence, serial fabrication techniques have been employed, such as ion track etching through glass [4] and laser machining fused silica [5] and Foturan photostructurable glass ceramics [6]. These methods have been used to realize high aspect ratio microfluidic devices [7] and planar patch-clamp electrodes [4] in glass materials. To avoid the use of specialized equipment, there has recently been an effort to adapt wafer-scale processing methods to glass, namely, reactive ion etching and lithographically-defined 'wet' etching. These methods have enabled the realization of a variety of devices including free–standing air cavities [2], micropumps [8], capillary electrophoresis microchambers [1, 9], high Q-factor resonators [10], microfluidic channels [11, 12], waveguides [13], bioanalytical devices [14] and single cell trapping wells [3], planar patch-clamp electrodes [15], and optical sensing platforms [1, 3].

Reactive ion etching is a major component of integrated circuit (IC) technology owing to its anisotropy and selectivity over masking and underlying layers [16]. Glass, however, shows an etch rate roughly an order of magnitude lower than silicon. As a result, relatively high biases are required when etching glass which compromises the masking material choice, smoothness of the etched surface, and attainable etch depth [17-20]. 'Wet' etching borosilicate and aluminosilicate glasses in hydrofluoric acid solutions show etch rates up to 8μm/min [8, 11, 21], but they exhibit isotropic etch profiles and frosted etched surfaces due to the presence of insoluble impurities [22]. Etching pure amorphous SiO_2, (fused silica/quartz), in contrast, results in optically transparent surfaces but the etch rate is on the order of 1 μm/min [3]. While methods have been developed to reduce the loss of optical clarity during borosilicate HF etching [21, 23], fused silica still has the advantage of chemical purity which makes it compatible with CMOS processing techniques [3] and eliminates substrate autofluorescence [24]. Previous masking film materials for fused silica have included chromium (Cr) [25], photoresists [13], polysilicon (polySi), amorphous silicon, aluminum, silicon nitride, and chromium/gold (Cr/Au) [3]. For example, fused silica was wet etched 60 μm deep with a Cr/Au mask in 49% HF for 1 hour [3] and 104 μm deep with a stress-reduced Cr mask in a heated buffered ammonium fluoride solution for 7 hours [25]. If fused silica etch depths substantially greater than 100 μm are desired, very long etching times and/or concentrated HF solutions (49% by mass) are required, which causes HF to

eventually migrate through most masking materials resulting in surface pitting and eventually mask deterioration and/or liftoff.

We report here a method to etch fused silica greater than 600 μm deep while keeping the substrate free of pits and maintaining a polished etched surface suitable for biological imaging, using an HF-resistant photosensitive resist (HFPR), ProTEK PSA (Brewer Science, Inc., Rolla, MO). ProTEK PSA is a negative tone resist system that consists of a thermoplastic cycloolefin copolymer which is a highly non-polar and hydrophobic polymer. A photosensitive agent induces crosslinking which renders it insoluble in hydrocarbon-based developing solvents. The minimal free volume of the cross-linked material, in addition to the abovementioned properties, minimizes the diffusion of polar HF molecules through the HFPR and thus renders it resistant to 49% HF [26, 27]. Undercut and mask deterioration are compared for substrates masked with the HFPR, Cr/Au, and polySi alone and Cr/Au and polySi films protected by the HFPR. Additionally, surface smoothness is compared for different etch depths. We demonstrate deep trenches in fused silica wafers using just the HFPR, obviating the need of furnaces or metal evaporators to deposit masking films for many etching applications. Even though etching 640 μm deep into a wafer approximately 650 μm thick, the surface of the resulting suspended membrane was smooth enough to allow fluorescence imaging without loss of image quality. Finally, we plasma etch pore arrays in the fused silica suspended membranes which may be used as planar patch-clamp electrode and/or suction electrode arrays.

2. Experimental details

2.1. Materials and substrate preparation

Square GE 124 fused silica wafers, 25.4 mm wide, 0.2 mm thick (Structure Probe Inc., West Chester, PA), 50 mm wide, 0.2 mm thick (Marc Optics Inc., Santa Ana, CA), and 50 mm wide, 0.55-0.65 mm thick (Quartz Scientific, Inc., Vancouver, WA) were used in this study. Photolithography and etching experiments were performed in class 100 and 1000 cleanrooms, respectively. All wafers were first cleaned in a piranha solution (3:1, 95% sulfuric acid: 30% hydrogen peroxide, General Chemical, Parsippany, NJ). The general process flow is shown in figure 1. For the gold masks, a 10 nm adhesion film of chromium and 200 or 240 nm of gold were evaporated with a Mark 40 Electron Beam Evaporator (CHA Industries, Fremont, CA). For polySi masks, approximately 1550 nm of polySi was deposited on both sides of the wafer in a low pressure chemical vapor deposition (LPCVD) tube furnace (Tyster Corporation, Torrance, CA) with the following parameters: 40 Pa (300 mT) pressure, 600°C deposition temperature, and 3 hour deposition time. The HF-resistant

photosensitive resist (HFPR), ProTEK PSA (Brewer Science, Inc., Rolla, MO), was photolithographically patterned according to the manufacturer's guidelines with a MA6 mask aligner (SUSS Microtec Ag, Garching, Germany). All wafers were patterned with pores 850–900 μm in diameter. Following development, wafers with the HFPR were further baked at 200°C for at least 10 minutes to ensure a highly cross-linked film due to the long HF exposure times used here. The opposite side of all wafers used in this study was blanket-protected with the HFPR to protect from HF vapor. AZ5214E photoresist (AZ Electronic Materials USA Corporation, Branchburg, NJ) and the HFPR were used to pattern the poly Si and Cr/Au films, respectively. Au and Cr were etched with Gold Etch Type TFA (Transene Company, Inc, Danvers, MA) and CR-7S Chromium Etchant (Cyantek Corporation, Fremont, CA) respectively. PolySi was etched in a SLR-770 deep reactive ion etcher (DRIE) (Oerlikon, Switzerland) with the Bosch process [28]. Table 1 summarizes the major equipment required for the processing of the different masking materials.

2.2. Fused silica wet etching

Fused silica was etched in 49% (by mass) hydrofluoric acid (General Chemical) in a custom-built polyethylene o-ring wafer holder (figure 1d). Following etching, the wafers were immediately immersed in water and then in a piranha solution to remove the HFPR. Au/Cr were removed in their respective etchants, while polySi was removed in a custom-built xenon difluoride (XeF_2) vapor etcher [29]. Wafer thicknesses before etching were measured with a micrometer or a Wyko NT3300 optical profilometer (Veeco Instruments, Inc, Plainview, NY). Etch depths were measured with a Dektak 6 stylus profilometer (Veeco Instruments) or Wyko NT3300 optical profilometer. Surface roughness was measured with the NT3300 profilometer in phase shift scanning interferometry mode.

2.3. Pore array device

For the devices with pore arrays, pores 20–50 μm in diameter were etched through suspended fused silica membranes (0.85 mm diameter, 6–13μm thick) in 0.2 mm thick wafers as previously described [15]. Briefly, a 10 nm titanium adhesion film and 450 nm nickel masking film were evaporated onto the wafer and electrochemically patterned in Class 10 85% phosphoric acid (General Chemical). The exposed fused silica was then etched in an Ulvac Neutral Loop Density 570 DRIE etching system with the following parameters: 52.0 A of current to the top and bottom electromagnetic coils, 30.6 A to the middle coil, 1000 W to the RF antenna, 90 W to the substrate electrode, 30 sccm C_3F_8, 0.4 Pa (3 mT) pressure, 50°C chamber temperature, 150°C shield temperature, and 20°C substrate electrode temperature. Twenty-one devices, 3.5 mm x 3.5 mm (length x width), were diced from a 25.4 mm x 25.4 mm wafer (American Precision Dicing, San Jose, CA).

2.4. Optical imaging of fluorescent neural tissue

Neural tissue from the medicinal leech *Hirudo verbana* was used for biological imaging experiments. A single midbody ganglion was isolated from the leech as previously described [30] and pinned to a polydimethylsiloxane (PDMS) slab. Auto-fluorescence from the ventral side of the ganglion was imaged with an upright microscope objective. For imaging through suspended fused silica membranes, the ganglion still attached to the PDMS slab was positioned ventral side down over the suspended membrane with a micromanipulator. Images were acquired with an inverted objective through fused silica surfaces that were HF etched 195 and 640 μm deep. Throughout the imaging experiments, tissue remained immersed in normal leech saline solution [31].

A custom dual upright and inverted microscope was used for imaging experiments. This system was constructed by attaching a modified Olympus upright BX WI microscope to an Olympus inverted IX51 microscope (Olympus America, Inc., Center Valley, PA) with a custom-built stage in between the two. A 5-W LED light (LedEngin, Inc., San Jose, CA) provided illumination at 460nm. The filter set comprised a 460/50 nm bandpass excitation filter, 505 nm dichroic mirror, and 510 nm long pass emission filter (Chroma Technology Corporation, Bellows Falls, VT). Images were recorded with an Olympus E420 digital camera.

3. Results and discussion

3.1. Integrity of masking materials in 49% HF

3.1.1 Chromium/gold + HFPR. Gold-chromium films have widely been used as a masking material for HF etching due to the chemical inertness of Au and the strong adhesion of Cr to glass and fused silica. With just Cr/Au as a mask for etching approximately 200 μm deep into fused silica, we were able to obtain an optically transparent etched surface, although the silica surface under the mask was severely pitted (figure 2a). Previous reports using a Cr/Au mask also showed similar pitting features [3]. However, when we further protected the Cr/Au film with the HFPR, the Cr/Au mask at the feature's edge was much better preserved even after almost 3 hours of etching time (166 μm deep). Pitting was also significantly reduced compared to the wafers masked with just Cr/Au mask (figure 2b).

3.1.2 Polysilicon + HFPR. To etch fused silica 600 μm deep we chose a polySi mask because it has been previously demonstrated to show substantially less pitting than Cr/Au [3]. However, our attempts to use a 1.5 μm thick polySi film were unsuccessful. As in previous reports, the polySi film remained defect free at 40 min of etching in 49% HF [3], but after 2 hours of etching defects in the polySi film developed, and after 5 hours we had to stop the

etch because the film was so pitted that HF solution leaked under the o-ring in the wafer holder (figure 2d). To resolve this problem, we patterned a single layer of the HFPR on the polySi film to protect it. This strategy allowed us to etch over 600 μm in fused silica, although after 9 hours of etching time, the polySi and fused silica underneath were significantly pitted. Additionally, the polySi at the edge of the patterned features had deteriorated (figure 2e), which sometimes caused polySi debris to fall onto the flat etching surface resulting in micromasking.

3.1.3 HFPR alone. We wanted to test the feasibility of using just a photoresist for deep HF etching. Fused silica wafers masked with the HFPR alone were etched approximately 200 and 600 μm deep (figure 2c, f). The HFPR never showed signs of being attacked by 49% HF. While there was significant undercut using the HFPR, the fused silica under the HFPR was not pitted even after 15 hours of etching (three consecutive etching steps on the same wafer). Furthermore, the etched surface remained polished and thus suitable for optical imaging.

3.2. Fused silica undercut and etch rates with different masking films

Masking with Cr/Au + HFPR resulted in etch rates of 1.12 ± 0.06 μm/min (mean ± standard deviation, N=7 wafers etched for 162–184 minutes; figure 3a). This rate corresponds to a final etch depth of 202 ± 11 μm in 3 hours. In contrast to the substantial variability of etch rates between wafers, etch rates were spatially very uniform within individual wafers: When two wafers were processed with a mask that defined multiple trenches, the depths of these trenches were constant to within 0.33 and 0.48 μm (root-mean-square variability of etch depth of 15 measured trenches in each of two wafers) after 166 minutes of etching. Etch rates were very similar when the HFPR was used alone, even though that resulted in much larger undercuts compared to the Cr/Au + HFPR when etching approximately 200 μm (figure 3a).

Since we were interested in fabricating thin membranes (see below), this variability in etch rate necessitated interrupting the etch process for intermediate depth measurements when we etched 600 μm deep features. PolySi + HFPR and the HFPR alone were used as masks to etch more than 600 μm deep. Compared to wafers masked with polySi + HFPR, undercut for wafers masked with the HFPR alone was much more extensive, extending all the way to the o-ring for these long etching times (figure 3b). The wafer for which a profilometry trace is shown in figure 3b was first masked with a 900 μm diameter feature and etched 390 μm deep. The wafer was then cleaned (to measure the etch depth), and the HFPR was patterned again, but with a 3.0 mm diameter feature aligned over the original 900 μm feature so as not to coat over the original undercut slope, and etched again in HF. The

reduced etch rate with the HFPR masked wafers compared to polySi + HFPR masked wafers for 600 μm deep etching (figure 3b) is likely caused by the extensive undercut with the HFPR alone combined with the increased etch depth: More fused silica is etched laterally, creating additional reaction products which must diffuse out before HF can diffuse into the mask opening.

3.3. Smoothness of etched surfaces

Etched surface roughness profiles were obtained from fused silica wafers using phase shift scanning interferometry [32]. Average roughness of etched surfaces versus etch depth are plotted in figure 4. There is no significant difference of surface roughness for different etch depths and/or different masking schemes. Because the average roughness cannot adequately capture all spatial aspects, representative three-dimensional roughness profiles are shown for surfaces etched to depths of 32, 166, and 645 μm in figure 5 to visualize defect patterns. To avoid any variability caused by different masking schemes, the comparison is only between the HFPR-masked wafers. The insets of figure 5 demonstrate that the spatial characteristics of these surfaces are similar regardless of etch depth. This suggests defect patterns may already be seeded on the surface in the first few minutes of etching. Because the surface roughness is very similar for a clean fused silica wafer and one patterned with the HFPR but not etched (figure 4), further investigations would be needed to determine if the origin of these defects are the result of mask patterning, surface defects in the native fused silica, and/or diffusion gradients in the liquid etching medium. In summary, we obtained surfaces with an average roughness under 10 nm at the bottom of 600 μm deep etched features, the deepest HF etching in fused silica reported to date.

3.4. Fluorescence imaging of biological tissue through the etched surfaces

To demonstrate that deep etching results in devices compatible with optical microscopy, we fluorescently imaged biological tissue through the fused silica surfaces. Neural tissue was imaged from above with an upright microscope objective (figure 6a). The same neural tissue was turned over and positioned over fused silica surfaces that were etched 195 and 640 μm deep (figure 6b, c). As seen in the figure, imaging through either of the etched surfaces with an inverted microscope objective did not negatively affect the image quality.

3.5. Pore arrays batch fabricated in suspended fused silica membranes

A fused silica wafer (188–195 μm thick) was etched in HF to a depth of 182 μm resulting in arrays of suspended membranes 6-13 μm thick (figure 7a). The Cr/Au + HFPR masking scheme was chosen for this device in order to minimize undercut (figure 3a) because of our relatively dense patterning (21 devices, each 3.5 x 3.5 mm wide, into a single 25.4 x 25.4

mm wafer). 20–50μm wide pores were plasma etched into the suspended membranes (figure 7a). Despite the density of the pores and thinness of the membranes, they were robust, and showed no signs of breakage or cracking when negative pressures up to 20 kPa were applied by means of a PDMS fluidic chamber (figure 7b) to immobilize biological tissue on the pore array (data not shown).

4. Conclusion

We have presented a processing scheme that can wet etch at least 600 μm deep into fused silica. We achieved this with a HF-resistant photosensitive resist, ProTEK PSA. This masking process, which does not require more than standard photolithography equipment (table 1), yielded substrates free of pits and etched surfaces with an average roughness on the order of 10 nm (figure 5) albeit with significant feature undercut. When the HFPR was combined with Cr/Au or polySi films, undercut was more limited with the tradeoff of substantial surface pitting for long etch times. In the future, it may be possible to minimize the surface pitting and undercut by combining the HFPR with stress-controlled 'hard' masks [21, 25].

We demonstrated that etched fused silica surfaces allow for optical imaging through the device. This processing scheme will contribute to the fabrication of transparent biological devices. One application is planar patch-clamp electrodes [4,15, 33]. Another is multielectrode arrays (MEAs)[34]: Perforated MEAs have received increased attention recently because they simultaneously enable tissue immobilization, oxygen perfusion, and recording from multiple electrodes in parallel, but currently available devices are not transparent [35, 36]. We are now able to fabricate similar devices in an optically transparent substrate that will allow for optical imaging [37]. Finally, due to the simplicity of pattering a photosensitive resist, researchers will be able to test the performance of a variety of fused silica and/or glass device prototypes in a minimal amount of processing time.

Acknowledgements

Funding for this work was provided by The Broad Foundations. DAW is the recipient of a Career Award at the Scientific Interface from the Burroughs Wellcome Fund. We thank James R. Heath for granting us use of his clean room facility and Habib Ahmad for contributions in creating figures in this manuscript. We also thank Jen-Kan Yu, Slobodan Mitrovic, and the UCLA Nanoelectronics Research Facility staff, especially Joe Zendejas and Tom Lee, for their support in device fabrication.

Table 1. Major processing equipment/steps required for processing masking materials.

	HFPR	Cr/Au	PolySi
Deposition	Spin-coater	Metal evaporator	LPCVD furnace
Pattering	UV Lithography	UV Lithography	UV Lithography
Pattern transfer	-	Cr/Au etchant	DRIE
Film removal	Piranha solution	Cr/Au etchant	XeF_2 (g)

Figure captions

Figure 1. General processing scheme for the HFPR patterning. A. Fused silica wafer after piranha cleaning. B. Wafer with a spin-coated masking film. C. Patterned feature in masking film. D. Patterned device in an o-ring holder. E. A masked fused silica wafer with an HF etched feature. F. A HF etched wafer that was piranha cleaned. See table 1 for major processing equipment.

Figure 2. Fused silica wafers etched in HF with different masks. A.) Wafers masked with Cr/Au alone, B.) Cr/Au combined with the HFPR, and C.) the HFPR alone were etched approximately 200 μm deep. Substrates masked with D.) polySi alone, E.) polySi combined with the HFPR, and F.) the HFPR alone were etched approximately 600 μm deep. Scale bars are 1 mm.

Figure 3. Profilometry traces of etched feature and etch rates for different masking schemes. A. Feature profiles of fused silica and etch rates after etching approximately 200 μm deep with a Cr/Au + HFPR mask (red) and the HFPR alone (blue). The aspect ratio (depth/patterned diameter) of the etched features is approximately 0.22. B. Feature profiles and etch rates of fused silica masked with a polySi + HFPR mask (green) and the HFPR alone (blue). Wafers masked with the HFPR alone were first etched 334–390 μm deep, piranha cleaned, and measured. Then the same etched wafers were patterned with the HFPR again and etched a second time to a total depth of 547–617 μm. The aspect ratio of the etched features is approximately 0.70. The orange structures above the profile traces represent the original mask pattern. Error bars represent the standard deviation of the etch rates from several wafers.

Figure 4. Average surface roughness of etched fused silica versus etch depth for several masking schemes. Surface roughness values in a 50 μm x 50 μm area are given for clean and HFPR patterned wafers (not etched) and HFPR only, Cr/Au only, Cr/Au + HFPR, and polySi + HFPR masked wafers that were etched in HF to different depths. Error bars represent the standard deviation of the average roughness measurements. Numbers above each data point correspond to the number of measured devices. The small data points for the polySi + HFPR masked wafers represent the two individual measurements.

Figure 5. Example surface profiles of etched fused silica. Phase shift scanning interferometry was utilized to visualize representative surface roughness features of wafers etched in HF that were masked with the HFPR alone. Substrates were etched A.) 32 μm deep, B.) 166 μm deep, and C.) 645 μm deep. Insets show detail at higher magnification.

Figure 6. HF etching fused wafers etched does not negatively affect image quality in fluorescence microscopy. A. Fluorescence image from neural tissue obtained with an upright microscope objective. B–C. Fluorescence image of the same neural tissue imaged with an inverted microscope objective through a fused silica membrane that was HF etched B.) 195 μm deep (an 8.2 μm thick suspended fused silica membrane) and C.) 640 μm deep (a 10–16.5μm thick suspended fused silica membrane).

Figure 7. Batch fabrication of through pore arrays in suspended fused silica membranes. A. Deep trenches etched with HF into a fused silica wafer (21 devices). Scale bar is 3.5 mm. Inset shows a single device (3.5 mm x 3.5 mm in length and width) diced from a wafer with a pore array that was plasma etched into the suspended fused silica membranes. Next inset shows a close up of the pore array fabricated into a thin suspended fused silica membrane. Scale bar is 100 μm. B. Schematic of a single pore array device interfaced to a PDMS fluidic chamber allowing negative pressure to be applied to immobilize biological tissue. Inset shows a cross section of a single device with a through pore array in the thin suspended membrane.

References

[1] Stjernström M, Roeraade J 1998 Method for fabrication of microfluidic systems in glass *Journal of Micromechanics and Microengineering* 8 33-8

[2] Baram A, Naftali M 2006 Dry etching of deep cavities in Pyrex for MEMS applications using standard lithography *Journal of Micromechanics and Microengineering* 16 2287

[3] Zhu H, Holl M, Ray T, Bhushan S, Meldrum D R 2009 Characterization of deep wet etching of fused silica glass for single cell and optical sensor deposition *Journal of Micromechanics and Microengineering* 19 065013

[4] Fertig N, George M, Klau M, Meyer C, Tilke A, Sobotta C, Blick R H, Behrends J C 2003 Microstructured apertures in planar glass substrates for ion channel research *Receptors & Channels* 9(1) 29-40

[5] Zimmer K, Braun A, Böhme R 2003 Etching of fused silica and glass with excimer laser at 351 nm *Applied Surface Science* 208-209 199-204

[6] Cheng Y, Sugioka K, Midorikawa K, Masuda M, Toyoda K, Kawachi M, Shihoyama K 2003 Control of the cross-sectional shape of a hollow microchannel embedded in photostructurable glass by use of a femtosecond laser *Optics letters* 28(1) 55-7

[7] Cheng Y, Sugioka K, Midorikawa K 2004 Microfluidic laser embedded in glass by three-dimensional femtosecond laser microprocessing *Optics letters* 29(17) 2007-9

[8] Bu M, Melvin T, Ensell G J, Wilkinson J S, Evans A G R 2004 A new masking technology for deep glass etching and its microfluidic application *Sensors and Actuators A: Physical* 115(2-3) 476-82

[9] Jacobson S C, Moore A W, Ramsey J M 1995 Fused quartz substrates for microchip electrophoresis *Analytical Chemistry* 67(13) 2059-63

[10] Corman T, Enoksson P, Stemme G 1998 Deep wet etching of borosilicate glass using an anodically bonded silicon substrate as mask *Journal of Micromechanics and Microengineering* 8 84-7

[11] Bien D, Rainey P, Mitchell S, Gamble H 2003 Characterization of masking materials for deep glass micromachining *Journal of Micromechanics and Microengineering* 13 S34-S40

[12] Iliescu C, Chen B T, Miao J M. Deep wet etching-through 1mm Pyrex glass wafer for microfluidic applications. Proceedings of the IEEE Twentieth Annual International Conference on Micro Electro Mechanical Systems, Vols 1 and 2 New York: IEEE; 2007. p. 762-5.

[13] Grosse A, Grewe M, Fouckhardt H 2001 Deep wet etching of fused silica glass for hollow capillary optical leaky waveguides in microfluidic devices *Journal of Micromechanics and Microengineering* 11 257-62

[14] Ray T, Zhu H, Meldrum D R 2010 Deep reactive ion etching of fused silica using a single-coated soft mask layer for bio-analytical applications *Journal of Micromechanics and Microengineering* 20 097002

[15] Nagarah J M, Paek E, Luo Y, Wang P, Hwang G S, Heath J R 2010 Batch Fabrication of High Performance Planar Patch Clamp Devices in Quartz *Advanced Materials* 22 4622-7

[16] Madou M. *Fundamentals of microfabrication: the science of miniaturization*: CRC press; 2002.

[17] Oehrlein G S, Zhang Y, Vender D, Joubert O 1994 Fluorocarbon high-density plasmas. II. Silicon dioxide and silicon etching using CF4 and CHF3 *Journal of Vacuum Science & Technology A-Vacuum Surfaces and Films* 12(2) 333-44

[18] Joubert O, Oehrlein G S, Surendra M, Zhang Y 1994 Reactive ion etching lag investigation of oxide etching in fluorocarbon electron-cyclotron-resonance plasmas *Journal of Vacuum Science & Technology A-Vacuum Surfaces and Films* 12(4) 1957-61

[19] Fukasawa T, Horiike Y 2003 Deep Dry Etching of Quartz Plate Over 100 m in Depth Employing Ultra-Thick Photoresist (SU-8) *Jpn J Appl Phys* 42 3702-6

[20] Kolari K 2008 Deep plasma etching of glass with a silicon shadow mask *Sensors and Actuators A: Physical* 141(2) 677-84

[21] Ceyssens F, Puers R 2009 Deep etching of glass wafers using sputtered molybdenum masks *Journal of Micromechanics and Microengineering* 19 067001

[22] Roach D H, Cooper A R 1986 Weakening of Soda Lime Glass by Particle Impact During Hydrofluoric Acid Etching *Journal of the American Ceramic Society* 69(7) C 153-C 5

[23] Iliescu C, Jing J, Tay F E H, Miao J, Sun T 2005 Characterization of masking layers for deep wet etching of glass in an improved HF/HCl solution *Surface and Coatings Technology* 198(1-3) 314-8

[24] Pokhriyal A, Lu M, Chaudhery V, Huang C S, Schulz S, Cunningham B T 2010 Photonic crystal enhanced fluorescence using a quartz substrate to reduce limits of detection *Optics Express* 18(24) 24793-808

[25] Steingoetter I, Fouckhardt H 2005 Deep fused silica wet etching using an Au-free and stress-reduced sputter-deposited Cr hard mask *Journal of Micromechanics and Microengineering* 15 2130-5

[26] Tang T, Planje C, Trichur R K, Zhong X F, Fowler S, Xu G, Yess K, Shao X, et al. Novel Polymeric Protective Coatings for Hydrofluoric Acid Vapor Etching During MEMS Release Etch *MAPS Device Packaging Conference 2010* (Scottsdale, AZ: IMAPS) p. 000076-80

[27] Tang T, Gu Xu R, Zhong X-F, Hong W, Flaim T D, Yess K, Trichur R K 2011 *US patent application* No 12/718516

[28] Jansen H, De Boer M, Unnikrishnan S, Louwerse M, Elwenspoek M 2009 Black silicon method X: a review on high speed and selective plasma etching of silicon with profile control: an in-depth comparison between Bosch and cryostat DRIE processes as a roadmap to next generation equipment *Journal of Micromechanics and Microengineering* 19 033001

[29] Chu P B, Chen J T, Yeh R, Lin G, Huang J C P, Warneke B A, Pister S Controlled pulse-etching with xenon difluoride *International Conference on Solid State Sensors and Actuators 1997* (Chicago, IL: IEEE) p. 665-8

[30] Kristan W B, Stent G S, Ort C A 1974 Neuronal control of swimming in the medicinal leech *Journal of Comparative Physiology A: Neuroethology, Sensory, Neural, and Behavioral Physiology* 94(2) 97-119

[31] Wagenaar D A, Hamilton M S, Huang T, Kristan W B, French K A 2010 A hormone-activated central pattern generator for courtship *Current Biology* 20(6) 487-95

[32] Conroy M, Mansfield D 2008 Scanning interferometry: Measuring microscale devices *Nature Photonics* 2(11) 661-3

[33] Pantoja R, Nagarah J, Starace D, Melosh N, Blunck R, Bezanilla F, Heath J 2004 Silicon chip-based patch-clamp electrodes integrated with PDMS microfluidics *Biosensors and Bioelectronics* 20(3) 509-17

[34] Wagenaar D, Pine J, Potter S 2006 An extremely rich repertoire of bursting patterns during the development of cortical cultures *BMC neuroscience* 7(1) 11

[35] Egert U, Okujeni S, Nisch W, Boven K H, Rudorf R, Gottschlich N, Stett A, editors. Perforated Microelectrode Arrays Optimize Oxygen Availability and Signal-to-Noise Ratio in Brain Slice Recordings. Mikrosystemtechnologie Kongress; 2005; Freiburg, Germany: VDE Verlag GmbH.

[36] Tonomura W, Moriguchi H, Jimbo Y, Konishi S 2010 Parallel multipoint recording of aligned and cultured neurons on micro channel array toward cellular network analysis *Biomedical Microdevices* 12(4) 737-43

[37] Baca S, Marin-Burgin A, Wagenaar D, Kristan W 2008 Widespread inhibition proportional to excitation controls the gain of a leech behavioral circuit *Neuron* 57(2) 276-89

Figure 1:

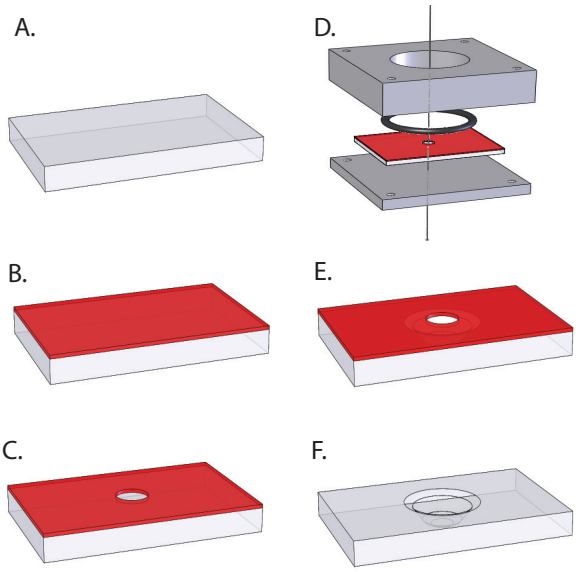

Figure 2:

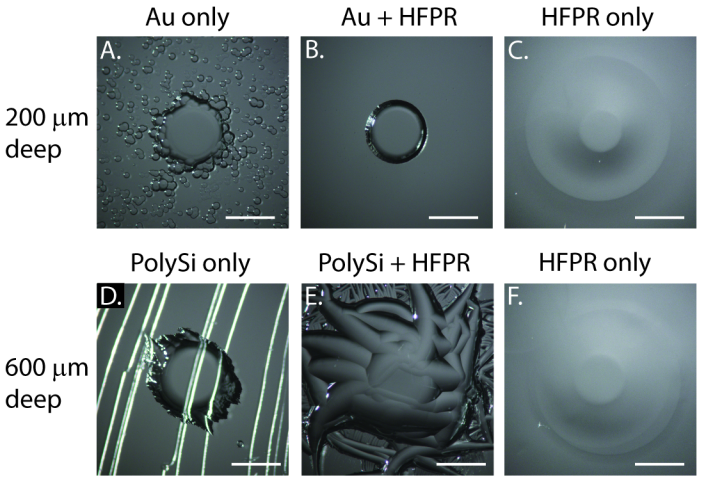

Figure 3:

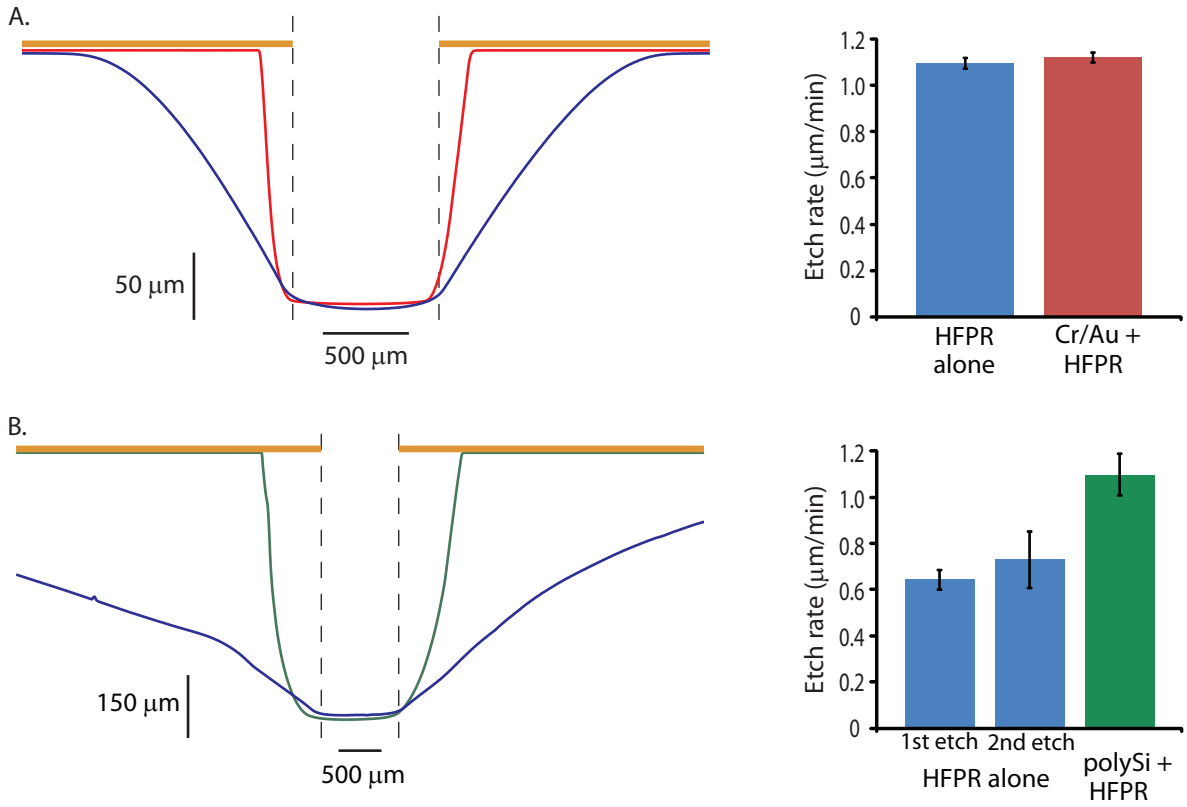
A.
50 μm
500 μm
B.
150 μm
500 μm
Etch rate (μm/min)
1.2
1.0
0.8
0.6
0.4
0.2
0
HFPR alone
Cr/Au + HFPR
Etch rate (μm/min)
1.2
1.0
0.8
0.6
0.4
0.2
0
1st etch
2nd etch
HFPR alone
polySi + HFPR

Figure 4:

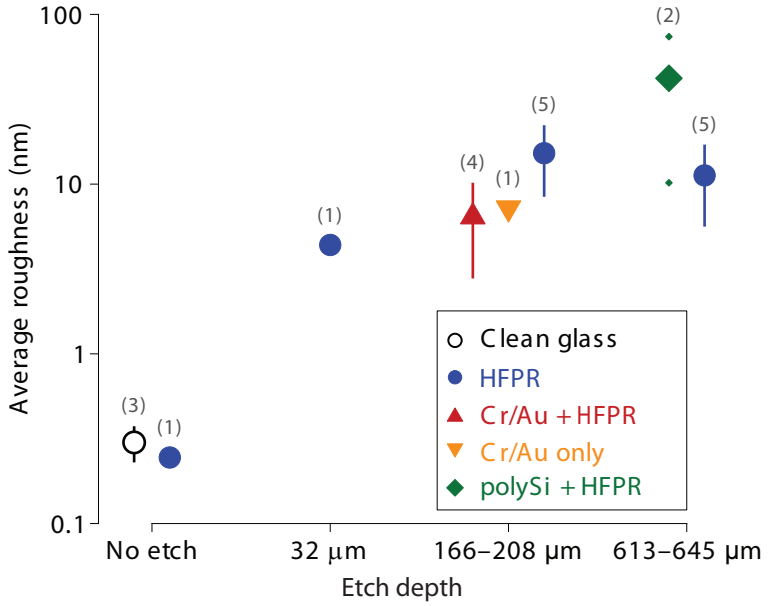

Figure 5:

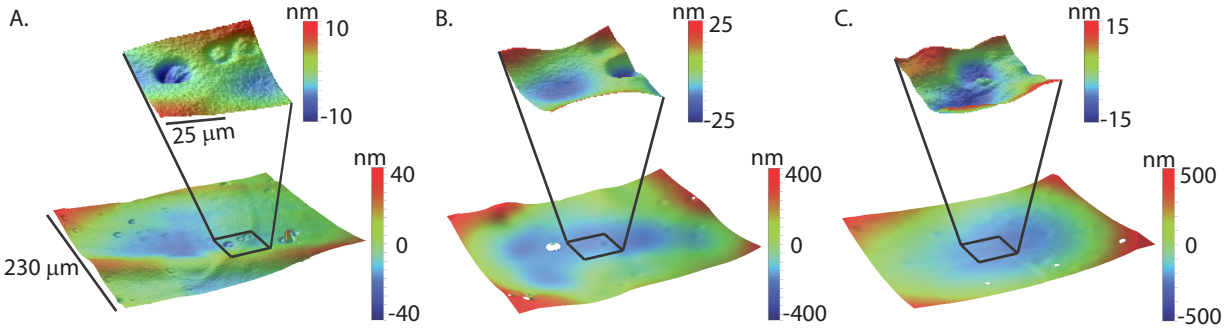

Figure 6:

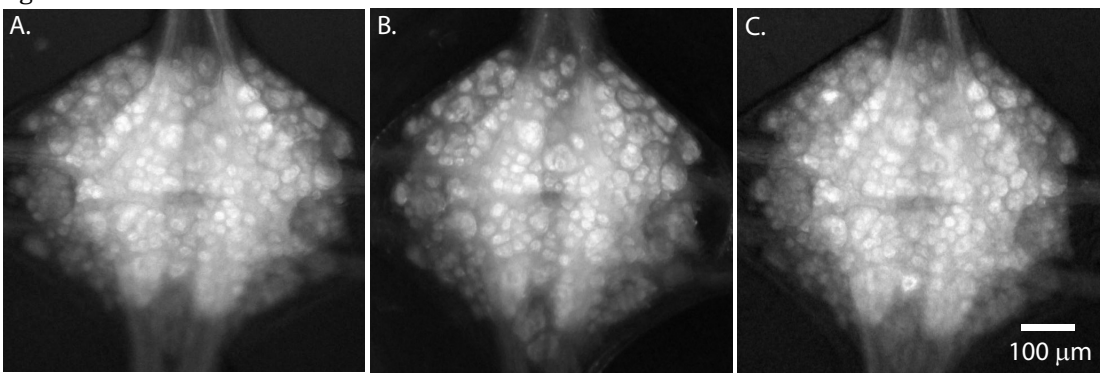

Figure 7: